Chinese Journal of
POLYMER SCIENCE

RESEARCH ARTICLE

https://doi.org/10.1007/s10118-026-3589-6
Chinese J. Polym. Sci.

Hydrophobicity Regulated Coacervate Droplet Size and the Thermal Protection Against Denaturation of Enzyme

Ming-Zhe Zhao[a], Kong-Ying Zhu[a,b], Xiao-Yan Yuan[a], and Li-Xia Ren[a*]

[a] *School of Materials Science and Engineering, Tianjin Key Laboratory of Composite and Functional Materials, Tianjin University, Tianjin 300350, China*
[b] *Analysis and Measurement Center, Tianjin University, Tianjin 300072, China*

Electronic Supplementary Information

Abstract Membrane-less organelles (MLOs), formed by liquid-liquid phase separation (LLPS) of biomolecules in cells, play crucial roles in cellular function such as gene expression, epigenetics, cellular metabolism, and so on. Moreover, the function of MLOs is closely related to the size of their droplets. Synthetic coacervates, which mimic MLOs, show great potential in cell biomimicry, drug delivery, and functioning as nanoreactors. However, the droplet size regulation of coacervates excluding concentration is challenging. In this work, synthetic coacervates are formed by poly(hydroxypropyl acrylate) (PHPA), which undergoes lower critical solution temperature (LCST)-type coacervation driven by hydrophobic interactions under physiological conditions. The size of the coacervate droplets is regulated by incorporating a more hydrophobic block, poly(di(ethylene glycol) ethyl ether acrylate) (PDEGA); the droplet size decreases from 5 μm to 234 nm as the PDEGA block length increases. Additionally, liquid-to-solid phase transition (LSPT) is observed with further increase in the PDEGA block. Thus, both droplet size and LSPT are controlled by the hydrophobicity of the block copolymers. The LCST-type coacervate shows thermal protection of enzymes such as glucose oxidase, which decreases as the size of coacervate droplets decreases, while the precipitates offer no protection activity. Furthermore, glucose oxidase (GOx) retains over 85% of its activity after 3 h of treatment at 60 °C with $PHPA_{44}$ coacervate. The hydrophobicity-tuned size control of coacervate droplets and LSPT bring insight into the molecular mechanism of coacervate phase change and facilitates the design of coacervate for biomimicking applications.

Keywords Block copolymer; Coacervate; Liquid-liquid phase separation; Liquid-to-solid phase transition; Protein thermal protection

Citation: Zhao, M. Z.; Zhu, K. Y.; Yuan, X. Y.; Ren, L. X. Hydrophobicity regulated coacervate droplet size and the thermal protection against denaturation of enzyme. *Chinese J. Polym. Sci.* https://doi.org/10.1007/s10118-026-3589-6

INTRODUCTION

Membrane-less organelles (MLOs), which are usually observed in eukaryotic cells, such as the nucleolus, stress granules, and processing bodies (P-bodies), can regulate various biological processes, including gene expression, protein translation, epigenetics, cellular metabolism, stress response, and cell signaling.[1,2] Moreover, MLOs have been reported to be associated with diseases such as neurodegenerative diseases.[3] Studies on MLOs and their mimics are crucial for understanding the function of cells and causes of certain diseases. Additionally, MLOs are considered to be related to the origin of life.[4] MLOs are generated by liquid-liquid phase separation (LLPS),[5] driven by weak and dynamic interactions among intrinsically disordered proteins (IDPs),[6] such as hydrophobic and electrostatic interactions and π-π stacking.[7,8] The LLPS, commonly termed as coacervation, plays a crucial role in preventing protein aggregation, regulating biochemical reactions, and mediating cellular signaling.[9,10] The design of artificial coacervates with well-defined architectures, capable of mimicking the structural and functional features of native MLOs, represents a promising approach for elucidating the molecular mechanisms underlying complex biological processes.

Researchers have synthesized various types of coacervates, including short peptides,[11,12] polypeptides,[13–15] host-guest supramolecular compounds[16] and synthetic polymers.[17–20] Stimuli-responsive coacervates, which form under stimuli such as pH,[12,21] temperature,[17–19,22] ion types,[23,24] ionic strength,[25–27] and crowding agents[28] have been extensively studied in artificial cells,[29] microreactors,[12,30] and drug delivery systems.[17,31,32] Beyond electrostatic and hydrophobic interactions, hydrogen bonding has recently been utilized to synthesize coacervate nanoparticles for bio-applications such as protocell mimicry [33] and osteoarthritis therapy.[34] In the preparation of coacervates, controlling droplet size is very important for the functionality of artificial cells.[5,35] In cells, the size of the nucleolus is closely related to its metabolic state,[36] and also affects the exchange rate between nucleolar components and the nucleoplasm.[37] For example, the efficiency of ribosome synthesis is correlated with the size of the nucleolus.[38] Thus, size control of coacervate droplets is critical, especially in the preparation of MLOs and artificial

* Corresponding author, E-mail: lxren@tju.edu.cn
Received November 18, 2025; Accepted January 25, 2026; Published online April 17, 2026

cells with specific functions. It has been demonstrated that the nucleolus undergoes dynamic size modulation that is controlled by the concentration of its components.[37,39] In addition, alternative strategies for modulating the coacervate droplet size have been actively investigated. Cui *et al*. reported the formation of hydrogen-bond-driven coacervates from poly(ethylene glycol) (PEG) and tannic acid (TA), where the droplet size was modulated by varying the PEG-to-TA mass ratio and pH.[33] Similarly, Ali *et al*. demonstrated the size modulation of coacervate droplets by mixing PEGylated and non-PEGylated peptides.[40] Chen *et al*. reported that the size of coacervate droplets formed by phosphorylated tau proteins was reduced by salt.[41] Xu *et al*. indicated that the presence of crowding agents results in the formation of larger coacervate complexes.[28] For these multicomponent coacervates, the droplet size is influenced by various factors in different systems.[42] To date, size control of coacervates composed of simple components has rarely been reported, and further studies on the molecular mechanism governing coacervate size control are essential for the design of LLPS-based materials.

Additionally, the dynamic responsiveness of coacervates is closely associated with biological processes and proteinopathies.[43,44] Coacervate droplets usually change dynamically and reversibly to exchange matter and energy under weak and transient interactions. However, it was found that Whi3 coacervate droplets underwent irreversible fibrillar precipitation upon prolonged incubation.[45] Such phase transitions from liquid-liquid to liquid-solid phase separation (usually termed as liquid-to-solid phase transition (LSPT)) of biomolecular condensates are closely related to the pathological acceleration of disease-causing mutations.[46] Studies have shown that the LSPT is closely linked to the pathogenesis of neurodegenerative diseases.[47,48] Understanding the molecular mechanisms underlying these transitions is crucial for both the development of cell mimicking biomaterials and the study of pathology of neurodegenerative diseases. However, the precise molecular mechanisms governing the LSPT remain unclear.

Poly(hydroxypropyl acrylate) (PHPA) is a thermoresponsive polymer with a lower critical solution temperature (LCST), which is influenced by the molecular weight.[49–51] However, the LLPS behavior of PHPA homopolymers and block copolymers remains unexplored. Herein, we studied the simple coacervation of PHPA homopolymers and block copolymers (PHPA-*b*-PDEGA) with the more hydrophobic poly(di(ethylene glycol) ethyl ether acrylate) (PDEGA) as the second thermoresponsive block under physiological conditions. The polymers underwent phase separation to form coacervate droplets above the LCST, and the size of the coacervate droplets decreased with increasing block length of PDEGA, and LSPT was observed with further increase in the PDEGA block. To better understand the potential biological applications of these coacervates, we evaluated their effect on the catalytic activity of glucose oxidase (GOx) under high-temperature conditions. Notably, 60%–80% of the GOx activity was retained under thermal stress in the presence of coacervates, which decreased with the coacervate droplet size. As the coacervate turned into a solid precipitate, there was almost no catalytic activity after thermal stress. The ability of coacervate droplets to modulate enzyme behavior in a size- and phase-dependent manner provides valuable insights into the molecular mechanisms and functional roles of biomolecular condensates in biological systems. Our study highlights the critical role of hydrophobic interactions in governing the size control and phase transitions of coacervates at the molecular level, which is essential for the rational design of coacervate-based materials with tunable biological functions.

EXPERIMENTAL

Materials

Hydroxypropyl acrylate (a mixture of 75% 2-hydroxypropyl acrylate and 25% 1-methyl-2-hydroxyethyl acrylate [HPA], ≥99.5%) and 4-cyanopentanoic acid dithiobenzoate (CPADB, 97%) were purchased from Macklin Biochemical Co., Ltd., (Shanghai, China). Di(ethylene glycol) ethyl ether acrylate (DEGA, 98%), ethylene glycol methyl ether acrylate (EGA, 98%), and Nile red (98%) were obtained from Tianjin Heowins Biochemical Technology Co., Ltd., (Tianjin, China). D-(+)-glucose (99%, anhydrous) and bovine serum albumin (BSA) were obtained from Aladdin Biochemical Technology (Shanghai, China). Glucose oxidase (GOx), horseradish peroxidase (HRP), and 10 mmol/L PBS buffer (pH=7.4) were supplied by Solarbio Science & Technology Co., Ltd., (Beijing, China). Sodium hydrogen phosphate (99.5%) and potassium dihydrogen phosphate (99%) were purchased from Bellingham Biochemical Technology Co., Ltd., (Beijing, China). Methylene blue was obtained from Sigma-Aldrich (St. Louis, MO, USA). 2,2′-Azobis(isobutyronitrile) (AIBN, Sigma-Aldrich, 99%) was purified by recrystallization from methanol. Deionized water was freshly prepared using a pure-water machine (DZG-303A, USA). All other reagents were acquired from Jiangtian Chemical Co., Ltd., (Tianjin, China).

Synthesis of Poly(hydroxypropyl acrylate) (PHPA)

PHPA was synthesized *via* reversible addition-fragmentation chain transfer (RAFT) polymerization (Scheme 1). A representative protocol for $PHPA_{44}$ preparation was conducted as follows: In a 10 mL Schlenk tube, CPADB (30.00 mg, 0.11 mmol), HPA (1.11 g, 8.54 mmol), and AIBN (2.94 mg, 17.90 μmol) were dissolved in 1,4-dioxane (1.65 mL). After three freeze-pump-thaw cycles, the tube was purged with N_2 and reacted at 70 °C for 3 h. The reaction was quenched by rapid cooling in liquid nitrogen and subsequent exposure to air. Unreacted monomers were removed *via* repeated ether precipitation. $PHPA_{25}$ and $PHPA_{60}$ were synthesized under identical conditions, but with adjusted [HPA]/[CPADB] ratios of 50/1 and 100/1, respectively. ^{1}H-NMR (800 MHz, $CDCl_3$, δ, ppm): 5.09–4.92 (br s, C<u>H</u>, poly(1-methyl-2-hydroxyethyl acrylate) side chain), 4.33–3.76 (br m, OC<u>H$_2$</u>C<u>H</u>, poly(2-hydroxypropyl acrylate) side chain), 3.72–3.50 (br m, C<u>H$_2$</u>,

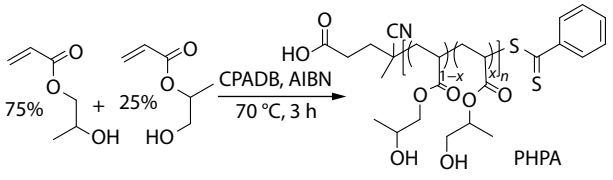

Scheme 1 Synthetic route to PHPA.

https://doi.org/10.1007/s10118-026-3589-6

poly(1-methyl-2-hydroxyethyl acrylate) side chain), 2.56–2.29 (br m, C<u>H</u>, PHPA backbone), 2.13–1.45 (br m, C<u>H</u>$_2$, PHPA backbone), 1.24–1.15(br s, C<u>H</u>$_3$, PHPA side chain).

Synthesis of Poly(hydroxypropyl acrylate)-*b*-poly(di(ethylene glycol) ethyl ether acrylate) (PHPA-*b*-PDEGA)

A typical protocol for the synthesis of PHPA$_{44}$-*b*-PDEGA$_{110}$ was as follows (Scheme 2). To a 10 mL Schlenk tube, PHPA$_{44}$ macro-CTA (58.60 mg, 9.77 μmol), DEGA (294.09 mg, 1.56 mmol) and AIBN (0.53 mg, 3.23 μmol) dissolved in 1,4-dioxane (1.65 mL) were added. The Schlenk tube was filled with N_2 after 3 freeze-pump-thaw cycles, and the mixture was reacted at 70 °C for 3 h. The Schlenk tube was quickly cooled in liquid nitrogen and quenched by opening it in air at the end of the reaction. The unreacted monomer was removed by repeated precipitation in *n*-hex. PHPA$_{44}$-*b*-PDEGA$_{110}$ was obtained as a pink solid after vacuum drying to a constant weight. Block copolymers with different chain lengths were prepared with different ratios of [DEGA]/[PHPA macro-CTA]. The same synthetic procedure was used to prepare the PHPA-*b*-PEGA. The degree of polymerization (DP) of the diblock copolymer was evaluated *via* ^{1}H-NMR spectroscopy by comparing the methylene proton signals from the side chains of PDEGA (δ=3.43–3.73 ppm) with those of the PHPA side chains (δ=5.09–4.92 ppm). ^{1}H-NMR (800 MHz, $CDCl_3$, δ, ppm): 4.27–4.13 (br s, $CO_2C\underline{H}_2$, PDEGA side chain), 3.75–3.46 (br m, $C\underline{H}_2OC\underline{H}_2C\underline{H}_2OC\underline{H}_2$, PDEGA side chain), 2.57–2.29 (br m, C<u>H</u>, PHPA, and PDEGA backbone), 2.13–1.45 (br m, C<u>H</u>$_2$, PHPA, and PDEGA backbone), 1.27–1.13 (br s, C<u>H</u>$_3$, PHPA, and PDEGA side chain).

Coacervate Preparation

The polymer was dissolved in PBS (10 mmol/L, pH=7.4) and incubated overnight at 4 °C. The polymer solution was heated to 35 °C to induce coacervation. We evaluated the pH-dependent and NaCl concentration-dependent stabilities of the coacervates by dissolving the polymer in 10 mmol/L PBS at pH values ranging from 6 to 8 and NaCl concentrations of 80–500 mmol/L. The resulting coacervate droplets were characterized using an optical microscope.

Coacervate Analysis

The polymer solution (c=20 mg/mL) was heated at 35 °C to induce coacervation or precipitation. Following incubation at 35 °C for 10 min, the coacervates/precipitates were separated by high-speed centrifugation. The supernatant was carefully removed, and the residual material was dried using filter paper. The relative water content was determined by calculating the ratio of the weight of freeze-dried coacervates/precipitates (m_1) to the weight of the unfreeze-dried coacervates (m_2). Polymer fraction = (weight of polymer in coacervate phase)/(total weight of polymer).

$$\text{Relative water content} = (m_2 - m_1)/m_2 \times 100\% \quad (1)$$

Encapsulation by Coacervate Droplets

Typically, PHPA$_{44}$-*b*-PDEGA$_{15}$ was dissolved in PBS at 4 °C and heated to room temperature. After that, 10 μL of Nile red solution (10 mg/mL in DMSO) was added to 200 μL of the PHPA$_{44}$-*b*-PDEGA$_{15}$ solution (20 mg/mL) and was vortexed for 30 s. Temperature was increased gradually from 25 °C to above 35 °C. Nile red encapsulated coacervate particles were observed under a green fluorescence channel using an inverted fluorescent microscope (DM2700M, Leica, Germany). For observation of protein encapsulation, fluorescein isothiocyanate (FITC)-tagged BSA and GOx were used. Methylene blue and FITC-labeled proteins were encapsulated in the same manner.

Encapsulation Efficiency of the Coacervate Droplets

To evaluate the encapsulation efficiency of Nile red, methylene blue, and fluorescently labeled proteins (FITC-BSA and FITC-GOx) within the coacervate droplets, polymer solutions containing the coacervates were incubated at 35 °C for 30 min and subsequently centrifuged at 8000 r/min to separate the supernatant. The concentrations of these agents in the supernatant were quantified using a UV-Vis spectrophotometer (GENESYS 180UV, Thermo Scientific, USA) at their respective maximum absorbance wavelengths. Standard calibration curves were established *via* UV spectrophotometry and were used to determine the residual mass of the encapsulated agents in the supernatant. The encapsulation efficiency of the coacervate droplets was determined by calculating the initial mass (m_0) of the encapsulated agent in the polymer solution and the residual mass (m_1) remaining in the supernatant.

$$\text{Encapsulation efficiency} = (m_0 - m_1)/m_0 \times 100\% \quad (2)$$

Measurement of the Relative GOx Activity

To investigate the thermal protection of coacervates on the activity of glucose oxidase (GOx), the enzyme was encapsulated in coacervate solutions at a concentration of 5 μg/mL (GOx) and 20 mg/mL (polymer), followed by incubation at 60 °C for 1, 2, or 3 h under controlled conditions. The heated GOx solutions were cooled to 4 °C, then diluted to the target concentration, and stored at this temperature until activity measurement. GOx activity was measured using a colorimetric assay as described in the literature.[52] In detail, 25 μL of diluted enzyme (100 ng/mL) was added to each well of a 96-well plate and mixed with 25 μL of 0.2 mol/L glucose dissolved in 10 mmol/L PBS. After a 10-min incubation at 30 °C, 50 μL of HRP (0.5 μg/mL) and 50 μL of 0.5 mmol/L 3,3',5,5'-tetramethylbenzidine (TMB) in 50 mmol/L citrate buffer (pH=5.5) were added. After 1 min, enzymatic activity was terminated by adding 20 μL of 1 mol/L sulfuric acid, and absorbance was measured at 450 nm using a microplate spectrophotometer. Untreated native GOx solutions were used as

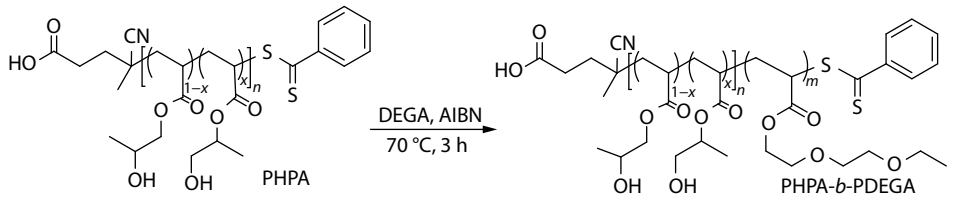

Scheme 2 Synthetic route to PHPA-*b*-PDEGA.

controls, and all thermally treated samples were analyzed in parallel under identical conditions. Relative GOx activity was calculated using Eq. (3):

$$\text{Relative GOx activity} = \frac{A_{450nm}(\text{sample}) - A_{450nm}(\text{negative})}{A_{450nm}(\text{positive}) - A_{450nm}(\text{negative})} \quad (3)$$

where A_{450nm}(sample), A_{450nm}(positive), and A_{450nm}(negative) represent the absorbance at 450 nm for the heat-treated GOx with polymer, native GOx without heat treatment, and sample without GOx, respectively.

Characterizations

Nuclear magnetic resonance (NMR) spectroscopy

^{1}H-NMR, variable-temperature NMR (VT-NMR), and ^{1}H-^{1}H nuclear Overhauser effect spectroscopy (NOESY) were performed on a Bruker AVANCE NEO spectrometer (800 MHz, Switzerland). For ^{1}H-NMR analysis, samples were dissolved in $CDCl_3$ (deuterated chloroform) and acquired at 25 °C. VT-NMR experiments involved dissolving the samples in 10 mmol/L PBS solution at 20 mg/mL, which were loaded into NMR tubes with a separate capillary containing D_2O (deuterium oxide) for lock signal stabilization. Temperature scans were conducted from 5 °C to 35 °C, with samples maintained at each temperature for 5 min to ensure thermal equilibrium, and water suppression was applied to the spectra. The variation of the main chain protons with temperature was analyzed by comparing the integrals of the main chain proton signals with those of the side chain protons at different temperatures. For the NOESY experiments, the samples were also scanned using the same method at 5 °C and 35 °C.

Gel permeation chromatography (GPC)

The molecular weights and molecular weight distributions of the PHPA homopolymer and the PHPA-*b*-PDEGA block copolymer were determined at 40 °C using an Agilent PL-GPC 50 system equipped with a refractive index detector. Tetrahydrofuran (THF) was used as eluent at a flow rate of 1.0 mL/min.

Cloud point temperature (T_{cp}) measurements

Turbidity measurements were carried out using a UV-Vis spectrophotometer (GENESYS 180UV, Thermo Scientific, USA) in a quartz cell with a diameter of 1 cm. The polymers were dissolved in PBS (10 mmol/L, pH=7.4) to a certain concentration and vortexed for 30 s to ensure complete dissolution and equilibration. The temperature of polymer samples was increased gradually from 4 °C to 60 °C. Transmittance was recorded as a function of temperature and measured at a wavelength of 600 nm. The LCST or T_{cp} is defined as the temperature at which the transmittance is 50%. A buffer solution without polymers was used as the reference.

Coacervate imaging

All the polymer solutions were observed using an optical microscope (DM2700M, Leica, Germany) equipped with a temperature-controlled stage (FDCS196, Linkam, UK). Before centrifugation, the coacervate solutions were mounted on a glass slide and covered with a coverslip. Images were captured 15 min after the initiation of coacervation.

Dynamic light scattering (DLS)

DLS measurements were performed on different polymer solutions at the required concentration in PBS at different temperatures using a Zetasizer Nano ZS90 (Malvern, UK). For each sample, three independent measurements were performed, with 11 consecutive scans per measurement, to ensure statistical robustness.

Statistical analysis

All experiments were performed in triplicate, and the results are presented as mean ± standard deviation (n=3). Significant differences were analyzed using one-way ANOVA, with p-values denoted as follows: $^*p<0.05$, $^{**}p<0.01$, and $^{***}p < 0.001$.

RESULTS AND DISCUSSION

Thermoresponsive Coacervation of PHPA

Thermoresponsive PHPA$_n$ (n representing degree of polymerization (DP)) with different DPs (n=25, 44, and 60) and narrow polydispersity indexes ($Đ$) were prepared by reversible addition-fragmentation chain transfer (RAFT) polymerization with CPADB as the chain transfer agent (Table S1 in the electronic supplementary information, ESI). The LCST behavior of the PHPA polymers under physiological conditions was studied to better fulfill bio-related applications. The LCST transition temperature (T_{cp}) in a phosphate buffer solution (PBS) was characterized by turbidity analysis, at which the transmittance was 50%.[53] T_{cp} is concentration- and DP-dependent. For PHPA$_{44}$, LCST-type phase separation is observed at concentrations of 5 mg/mL and higher (Fig. S1 in ESI). The T_{cp} decreases with an increase in PHPA$_{44}$ concentration, with a smaller decrease observed at concentrations of 15 mg/mL (32 °C) and 20 mg/mL (31 °C) (Figs. 1a and 1b). T_{cp} also decreases with increasing DP of the PHPA$_n$ polymers, as depicted in Fig. S2 (in ESI). LCST phase transition cannot be observed at DP of 25 at 20 mg/mL, whereas the T_{cp} dropped to 27 °C at DP of 60. The concentration- and DP-dependent LCST might be attributed to the enhanced inter-/intra-macromolecular interactions at higher concentrations and DPs, which is a typical characteristic of LCST-type polymer aqueous solutions.[54,55]

It is noted that the PBS solution of PHPA$_{44}$ phase-separated into polymer-poor and polymer-rich liquid phases at temperatures higher than the LCST after centrifugation (inset in Fig. 1a), which is a typical characteristic of the coacervates formed by LLPS. As shown in Fig. 1(c) and Movie S1 (in ESI), micrometer-sized spherical droplets with smooth surfaces are fused to verify the LLPS phenomenon. The coacervate morphology and liquid-like structure were further characterized by confocal laser scanning microscopy (CLSM) and fluorescence recovery after photobleaching (FRAP) (Figs. S3 and S4 in ESI). The fluorescence intensity of the photobleached droplets recovers rapidly (Fig. S4 in ESI), reaching 84% of its initial intensity within 30 s. This demonstrates the liquid-like nature of PHPA$_{44}$ coacervate droplets formed by LLPS.[12,16,23,56,57] The coacervation of PHPA$_{44}$ is both temperature- and concentration-dependent, as shown in the phase diagram (Figs. 1b and 1d). As shown in Fig. 1(d), the solution remains homogeneous and no droplets can be observed at 1 mg/mL, even at 50 °C. When the concentration increases to 5 mg/mL and the temperature exceeds its T_{cp} (49.5 °C), coacervation droplets can be observed in Fig. 1(d). At concentrations above 10 mg/mL, coacervation can be observed at temperatures higher than 35 °C (Fig. 1d). No coacervate droplets can be observed when the temperature and concentration were within the white region, as shown in Fig. 1(b). This indi-

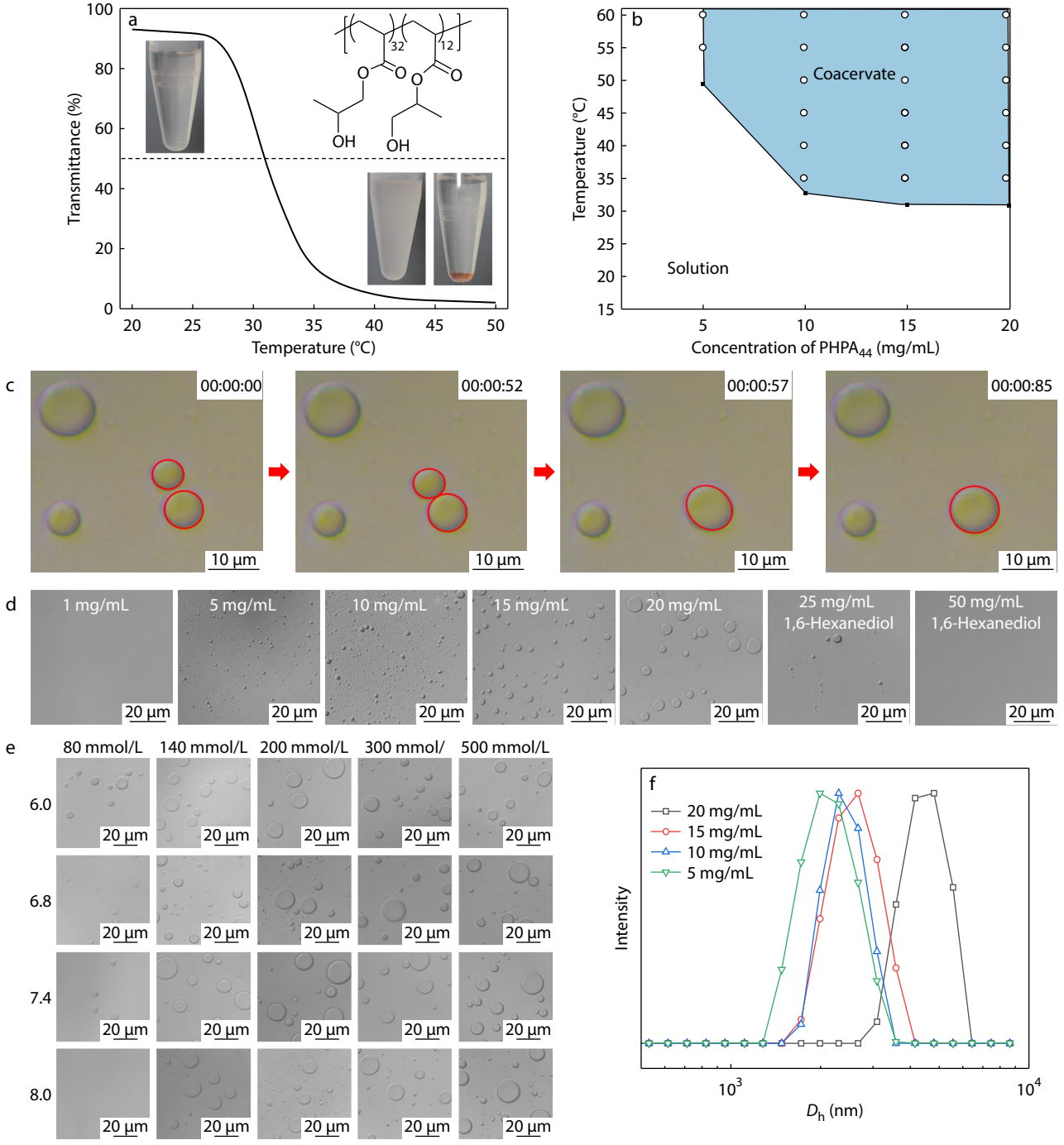

Fig. 1 Temperature-dependent coacervation of $PHPA_{44}$ solutions. (a) Temperature-dependent transmittance of 20 mg/mL $PHPA_{44}$ in PBS. Insets show optical photographs of transparent and turbid solutions. The turbid solution separated into two phases after centrifugation. (b) Phase diagram of $PHPA_{44}$ in PBS: temperature versus polymer concentration; (c) Fusion of $PHPA_{44}$ coacervate droplets (20 mg/mL, 35 °C) (red circles highlight fusion events, see Movie S1 in ESI); (d) Optical microscopic images of coacervate droplets of 1, 5, 10, 15 and 20 mg/mL $PHPA_{44}$, as well as 20 mg/mL $PHPA_{44}$ droplets supplemented with different concentrations of 1,6-hexanediol at 50 °C; (e) Optical microscopy images of $PHPA_{44}$ (20 mg/mL) in 10 mmol/L phosphate buffer at varying NaCl concentrations and pH values; (f) Size distributions of 5, 10, 15 and 20 mg/mL $PHPA_{44}$ in PBS at 50 °C measured by DLS.

cates that the LLPS behavior of $PHPA_{44}$ is analogous to that of IDPs,[5,7] occurring only when both the critical concentration and critical temperature are exceeded. As reported, some coacervates prepared from either neutral or charged compounds are sensitive to pH and salt[21,58–60] limiting their applications under physiological conditions. We studied the stability of $PHPA_{44}$ coacervates at different pH values and NaCl concentrations, while maintaining the same phosphate concentration as in PBS.[31] As depicted in Fig. 1(e), coacervation is observed at NaCl concentrations higher than 80 mmol/L

https://doi.org/10.1007/s10118-026-3589-6

from pH=6 to pH=8 at 35 °C. Notably, coacervate droplets are absent only at pH 8 (80 mmol/L NaCl), which may be attributed to the protonation of carboxylic acid groups in the chain transfer agent. Hence, coacervates prepared using neutral PHPA polymers are stable under physiological conditions and show minimal sensitivity to pH and salt concentration, making them well-suited for biological applications.

For LCST-type coacervation of PHPA polymers, hydrophobic interactions have been proposed as the driving force for LLPS. To verify this, 1,6-hexanediol, an amphiphilic compound reported to disrupt coacervates formed *via* hydrophobic interactions,[7,61,62] was used in this work. As shown in Fig. 1(d), 1,6-hexanediol significantly reduces the size of $PHPA_{44}$ coacervate droplets (20 mg/mL) at 25 mg/mL, while complete disruption occurred at 50 mg/mL. These results strongly indicate that hydrophobic interactions drive LLPS of $PHPA_{44}$ macromolecules under physiological conditions.

As shown in Fig. 1(f), the size distributions of the different concentrations were studied using DLS. Consistent with optical microscopy observations (Fig. 1d), the droplet size increases with increasing concentration. The size distribution shows that the average droplet diameter gradually increases from about 2 μm (5 mg/mL) to about 5 μm (20 mg/mL) in PBS (Fig. 1f). A similar phenomenon can be observed for $PHPA_{60}$, as shown in Fig. S5 (in ESI), as the droplet size increases with the polymer concentration, which is consistent with previously reported coacervates.[7,33] Research into the size of coacervate droplets is crucial for applications in fields such as nanomedicine and catalysis.[63] For example, the size and distribution of drug carriers can influence the *in vivo* drug distribution and cell uptake efficiency.[64,65] Additionally, in cell biomimicking, the size of MLOs is closely related to their function and metabolism.[37,38] Therefore, it is of great importance to design coacervates with well-controlled droplet size. Although droplet size can be tuned by changing the concentration, this approach is often impractical because of the high osmotic pressure and toxicity at elevated concentrations. Therefore, controlling the size of coacervate droplets through molecular design remains a challenge.

Size Control and LSPT *via* Hydrophobic Second Blocks

To further study the effects of hydrophobic interactions and the degree of hydrophobicity on the phase transition behavior of PHPA polymers in PBS, thermoresponsive poly(di(ethylene glycol) ethyl ether acrylate) (PDEGA) blocks, which are more hydrophobic than PHPA, were introduced to prepare the PHPA-*b*-PDEGA block copolymers.

As shown in Fig. 2 and Table S1 (in ESI), a series of $PHPA_{44}$-*b*-$PDEGA_m$ (*m*=0, 15, 40, 50, 66, 85, 110, and 140) block copolymers with increasing DP values of the PDEGA blocks were synthesized *via* sequential RAFT polymerization. As a reference, a $PDEGA_{60}$ homopolymer was prepared. It was noted the $PDEGA_{60}$ homopolymer formed solid precipitates in PBS at temperatures higher than LCST (10 °C) (Fig. S6 in ESI), thereby verifying the hydrophobic nature of the PDEGA block.[50,66] The T_{cp} of the polymers in PBS was calculated by turbidity analysis and decreased with increasing PDEGA block length (Figs. 3a and 3b). Compared with $PHPA_{44}$, for which the T_{cp} was 31 °C, the T_{cp} of $PHPA_{44}$-*b*-$PDEGA_{15}$ decreased to 26 °C. With a further increase in PDEGA block length, T_{cp} continued to decrease, as the T_{cp} for $PHPA_{44}$-*b*-$PDEGA_{140}$ was only 6 °C. Hence, hydrophobic interactions at temperatures higher than the LCST were gradually enhanced with increasing PDEGA block length. The hydrophobic interactions and phase transition temperature can be flexibly tuned by changing the DP of the PDEGA block, which is beneficial for the systematic study of the influence of hydrophobic interactions on the phase separation behavior of the polymer in PBS.

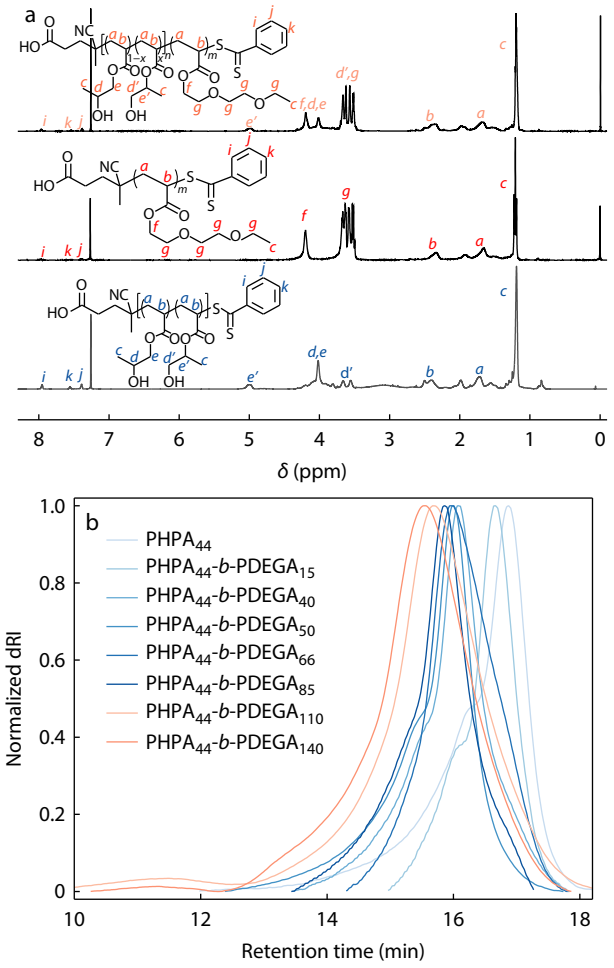

Fig. 2 (a) ^{1}H-NMR spectra of $PHPA_{44}$ (bottom), $PDEGA_{60}$ (middle) and $PHPA_{44}$-*b*-$PDEGA_{40}$ (top) recorded in $CDCl_3$; (b) GPC traces of $PHPA_{44}$ and $PHPA_{44}$-*b*-$PDEGA_m$ block copolymers.

The coacervation of $PHPA_{44}$-*b*-$PDEGA_m$ copolymers in PBS at neutral pH was studied. As shown in Figs. 3(c) and 3(d) and Fig. S7 (in ESI), coacervate droplets with circular shapes and smooth surfaces can be observed at temperatures above the LCST, when the DP of the PDEGA block ranged from 15 to 85 at 20 mg/mL. A similar droplet fusion was observed, as shown in Fig. 3(c) and Movie S2 (in ESI), confirming the occurrence of LLPS. FRAP results (Fig. S8 in ESI) shows that the fluorescence signal of $PHPA_{44}$-*b*-$PDEGA_{15}$ recovered to 84% at 70 s, demonstrating the liquid-like nature of the coacervate solution. However, when the DP of PDEGA was 110, irregular precipitates appeared (Fig. 3d), indicating the transition from LLPS to LSPT. Fig. S9 (in ESI) shows the optical images of all the samples after centrifugation at 35 °C, showing a distinct interface separating the supernatant layer from the dense polymer-rich

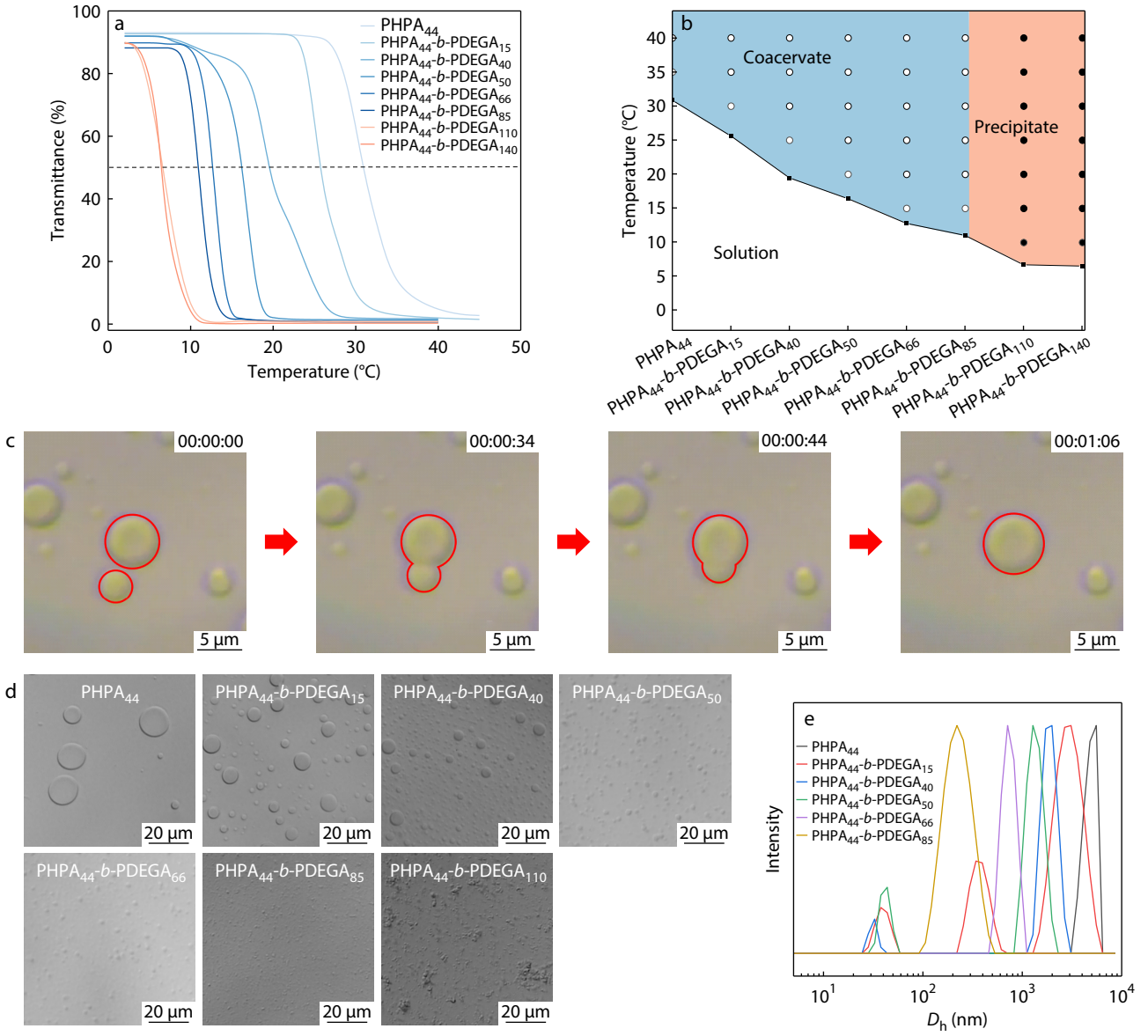

Fig. 3 Temperature-dependent coacervation of $PHPA_{44}$-*b*-$PDEGA_m$ in PBS. (a) The temperature-dependent transmittance of 20 mg/mL $PHPA_{44}$-*b*-$PDEGA_m$ solution; (b) Phase diagram of $PHPA_{44}$-*b*-$PDEGA_m$ in PBS: temperature versus PDEGA block DP; (c) Fusion of $PHPA_{44}$-*b*-$PDEGA_{15}$ coacervate droplets (20 mg/mL, 35 °C) (red circles highlight fusion events, see Movie S2 in ESI); (d) Optical microscopic image of coacervate droplets of $PHPA_{44}$-*b*-$PDEGA_m$ (*m*=0, 15, 40, 50, 66, and 85) and $PHPA_{44}$-*b*-$PDEGA_{110}$ solid precipitates at 20 mg/mL and 35 °C; (e) Size distributions of $PHPA_{44}$-*b*-$PDEGA_m$ (*m*=0, 15, 40, 50, 66, and 85) coacervates in PBS at 20 mg/mL and 35 °C measured by DLS.

phase. LLPS was observed at a PDEGA DP of 85, whereas solid precipitates were formed at a higher DP. Therefore, the formation of coacervates and precipitates was controlled by the DP of the hydrophobic PDEGA block, as shown in Fig. 3(b). Furthermore, the dilution of $PHPA_{44}$-*b*-$PDEGA_{40}$ from 20 mg/mL to 5 mg/mL in PBS decreased the coacervate droplet size (Fig. S10 in ESI), which was similar to the behavior observed for $PHPA_{44}$. Even at a higher concentration of 40 mg/mL, LLPS can be observed, with the polymer-rich dense phase occupying a larger volumetric proportion than the solution at 20 mg/mL (Fig. S11 in ESI). Notably, with increasing PDEGA block length, the size of the coacervate droplets decreases sequentially, as shown in Fig. 3(d). The droplet size of the coacervate was studied using DLS, as shown in Fig. 3(e). The hydrodynamic diameter (D_h) gradually decreases from about 5 μm ($PHPA_{44}$) to about 234 nm ($PHPA_{44}$-*b*-$PDEGA_{85}$) with an increase in the PDEGA block (Table S1 in ESI). And, the stability of coacervate droplets was studied by capturing images of the coacervate solution after incubation at 35 °C for 4 h. As shown in Fig. S12 (in ESI), the coacervate droplets can clearly be observed with clear boundaries to verify the stability of the coacervate droplets, which shows potential for drug delivery.

It has been reported that the coacervate phase typically retains a high water content owing to incomplete dehydration above the LCST, which is critical for protecting the encapsulated labile molecules.[12,18,23,58] The relative weight percent of water in dense coacervate layers (Fig. 4a) and the relative

https://doi.org/10.1007/s10118-026-3589-6

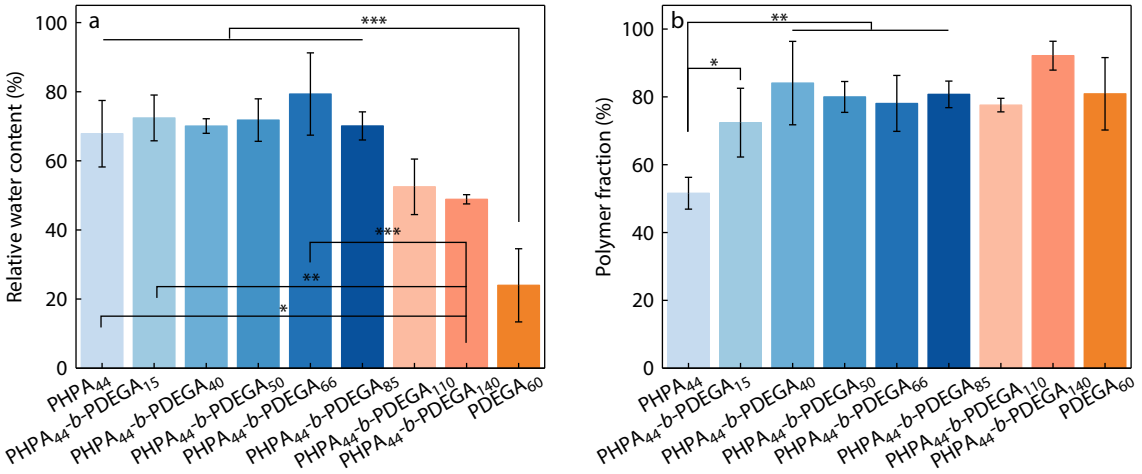

Fig. 4 (a) Relative water content and (b) polymer fraction of PHPA$_{44}$-*b*-PDEGA$_m$ (*m*=0,15, 40, 50, 66, 85, 110, and 140) with PDEGA$_{60}$ as reference, $^{*}p<0.05$, $^{**}p<0.01$, and $^{***}p < 0.001$.

polymer fraction in coacervate (Fig. 4b) were calculated respectively after freeze-drying. The relative water contents of the PHPA$_{44}$ and PHPA$_{44}$-*b*-PDEGA$_{66}$ coacervates were calculated to be about 68% and about 79%, respectively, indicating abundant water molecules in the PHPA-based coacervates. However, the incorporation of excessive PDEGA led to precipitation and a decrease in the relative water content below 50%. Additionally, PDEGA incorporation promotes polymer separation from the dilute phase into the dense coacervate phase/precipitate. For example, the polymer fraction was only 51% in the PHPA$_{44}$ coacervates, increased to 71% in the PHPA$_{44}$-*b*-PDEGA$_{15}$ coacervates, and the highest polymer precipitation was observed in the PHPA$_{44}$-*b*-PDEGA$_{140}$ precipitates (92%).

To further verify that the coacervate droplet size and phase transition behavior were controlled by hydrophobicity, two series of PHPA$_{60}$-*b*-PDEGA$_x$ (*x*=30, 50, 60, 100, and 160) and PHPA$_{25}$-*b*-PDEGA$_y$ (*y*=10, 35, 55, and 75) copolymers were prepared (Table S1 in ESI). The corresponding phase diagrams are shown in Figs. S13 and S14 (in ESI), respectively. For PHPA$_{60}$-*b*-PDEGA$_x$, the coacervate droplet size gradually decreased from about 5 μm to about 236 nm as the PDEGA DP increased from 0 to 100 (Figs. S13c and S13d in ESI), whereas precipitation occurred at a DP of 160 (Table S1, Figs. S13b and S13c in ESI), which is similar to the behavior of PHPA$_{44}$-*b*-PDEGA$_m$. For the PHPA$_{25}$-*b*-PDEGA$_y$ series, introducing a short PDEGA$_{10}$ block rendered the polymer solution thermally responsive, forming coacervates at temperatures higher than the LCST with a droplet size of approximately 3 μm (Fig. S14 and Table S1 in ESI). With a further increase in the PDEGA block length, the droplet size decreased (Figs. S14c and S14d in ESI). Moreover, similar to the PHPA$_{44}$-*b*-PDEGA$_m$ series, the relative water content was reduced, while the polymer fraction increased in the coacervate or precipitated phase with the incorporation of PDEGA (Fig. S15 in ESI).

Furthermore, to validate the role of hydrophobicity in tuning the droplet size and phase transition, we incorporated a thermally stable and more hydrophobic poly(ethylene glycol methyl ether acrylate) (PEGA) as the hydrophobic block to prepare PHPA$_{60}$-*b*-PEGA$_n$ (*n*=20, 150, Fig. 5a, Table S1 in ESI)

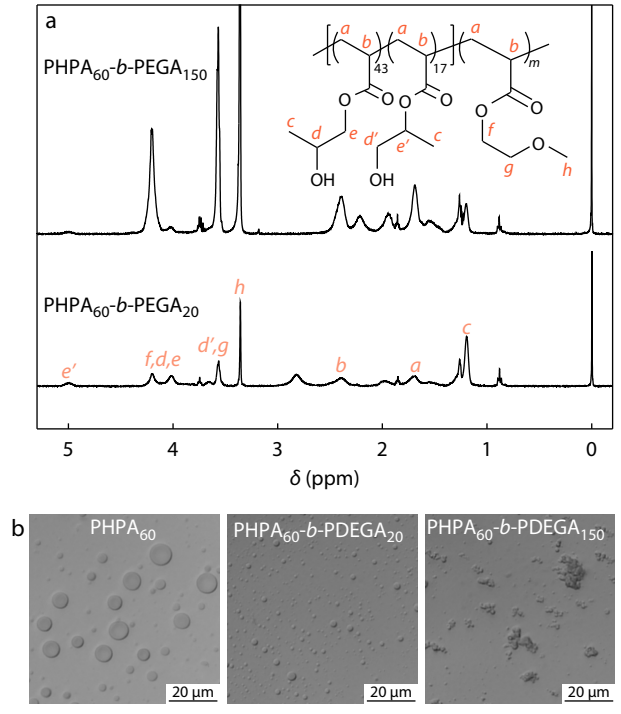

Fig. 5 (a) ^{1}H-NMR spectra of PHPA$_{60}$-*b*-PEGA$_{20}$ (bottom) and PHPA$_{60}$-*b*-PEGA$_{150}$ (top) in $CDCl_3$; (b) Optical microscopic images of coacervate droplets of PHPA$_{60}$-*b*-PEGA$_m$ (*m*=0, 20) and PHPA$_{60}$-*b*-PEGA$_{150}$ solid precipitates (20 mg/mL in PBS, 35 °C).

block copolymers. As previously reported, PEGA is more hydrophobic than PDEGA.[50,67] It was found that PHPA$_{60}$-*b*-PEGA$_{20}$ formed coacervates at room temperature that were insensitive to temperature due to the thermal stability and hydrophobicity of the PEGA block. The average droplet size of the coacervate was approximately 856 nm, which is significantly smaller than that of PHPA$_{60}$ (about 5 μm) (Table S1, Fig. 5b and Fig. S16 in ESI). At a PEGA DP of 150, the block copolymer precipitated from the PBS, resulting in a liquid-to-solid phase transition. Collectively, these results demonstrated that the droplet size and liquid-to-solid phase transition could be

tuned by modulating the polymer hydrophobicity through the incorporation of a more hydrophobic second block, regardless of the thermal responsiveness.

The hydrophobicity-tuned coacervate droplet size and liquid-to-solid phase transition were further studied using temperature-dependent ^{1}H-NMR and 2D nuclear Overhauser effect spectroscopy (NOESY) to explore the molecular mechanisms. The ^{1}H-NMR spectra presented in Figs. 6(a)–6(c) were recorded from 5 °C to 35 °C in PBS at an interval of 5 °C between each spectrum. With increasing temperature, all proton signals shifted to the low-field region, which was consistent with previous reports.[17,22,68] As shown in Fig. 6(a), at 35 °C (above the T_{cp} of $PHPA_{44}$), the signal intensities and integrated areas of both main chain and side chain remained almost unchanged compared to those below T_{cp}, indicating sufficient chain mobility and hydration above LCST.[17,22,68] This result is consistent with the LLPS-driven coacervate formation. In contrast, for $PDEGA_{60}$ (Fig. 6b), the integrated area of the main chain proton signals decreased gradually above T_{cp}, demonstrating the aggregation of the polymer due to the liquid-to-solid phase transition. Quantitative analyses of the integration of proton signals from the methylene groups in the main chain *vs* temperature (Fig. S17 in ESI) shows that the integration is dramatically decreased to 27% for $PDEGA_{60}$ precipitates, while the liquid-like $PHPA_{44}$ is more than 90%. It is noted that A broad peak near the terminal methyl groups of $PDEGA_{60}$ is observed at 25 °C and above, likely corresponding to methyl groups in aggregation phase, which are probably partially swollen precipitates. With a further increase in temperature, the area of the original methyl signal decreased, while the broad peak increased, confirming enhanced solid phase aggregation. Quantitative analyses revealed that approximately 81% of the PDEGA was in the aggregation phase, which is in agreement with the polymer fraction shown in Fig. 4(b). Additionally, the ethylene glycol proton signals broadened and lost their fine splitting structure, indicating strong hydrophobic interactions among the polymer side chains.[69]

For $PHPA_{44}$-*b*-$PDEGA_{40}$ coacervate, all proton signals were sharp and well-split below T_{cp} (19 °C) (Fig. 6c), indicating a homogeneous solution. Similar results were observed from NOESY spectrum at 5 °C (Fig. 6d). The ^{1}H-^{1}H nuclear Overhauser effect (NOE) signal primarily reflects the spatial proximity between protons, with an interaction range of less

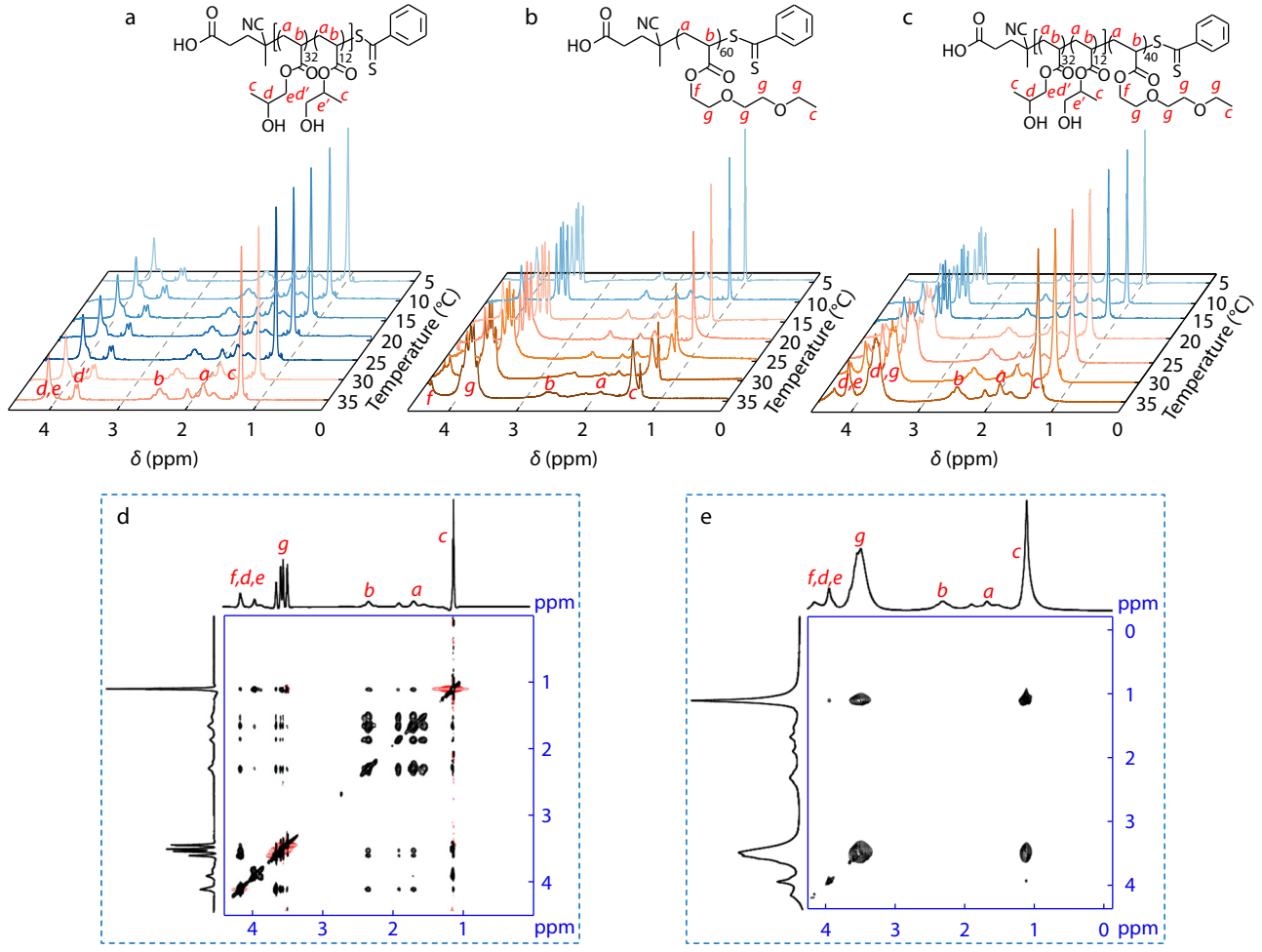

Fig. 6 ^{1}H-NMR spectra of (a) $PHPA_{44}$ (b) $PDEGA_{60}$ solid precipitate, and (c) $PHPA_{44}$-*b*-$PDEGA_{40}$ coacervate recorded as a function of temperature in PBS. D_2O was added to the capillary tube as the deuterium lock solvent for field stability. The 2D ^{1}H-^{1}H NOESY spectra of $PHPA_{44}$-*b*-$PDEGA_{40}$ in PBS at (d) 5 °C (below T_{cp}) and (e) 25 °C (above T_{cp}).

https://doi.org/10.1007/s10118-026-3589-6

than 0.5 nm,[69,70] making it a powerful tool for detecting weak interactions. Cross-peaks corresponding to interactions among the main chains, side chains, and between the main and side chains can be clearly observed (Fig. 6d), indicating a dynamic coil conformation of the polymer in PBS. However, at 20 °C and above, ethylene glycol signals broadened into a single peak (Fig. 6c), demonstrating strong interactions and partial aggregation of the PDEGA block. A weaker broad shoulder emerged near terminal methyl protons at 25 °C and above, coinciding with the partial aggregation of PDEGA block as well. In Fig. 6(e), cross-peaks associated with the main chain protons disappeared, while those between PDEGA side chain protons (H-*g* and H-*c*) dominated, indicating tight packing (<0.5 nm) of the PDEGA side chains *via* strong hydrophobic interactions. Compared to the $PHPA_{44}$ coacervate solution (Fig. 6a), both inter- and intra-molecular hydrophobic interactions were enhanced by the PDEGA block, likely forming compact microdomains, as shown in Scheme 3, reducing the coacervate droplet size. With increasing PDEGA block length, the enhanced hydrophobic interactions promoted the formation of more compact PDEGA-rich microdomains within the coacervate droplets, which restricted the droplet fusion kinetics and fluidity (Figs. 1c and 3c, Figs. S4 and S8 in ESI), thereby maintaining smaller droplet sizes in the system. Meanwhile, the hydrated PHPA blocks stabilized the hydrophobic microdomains and droplet interface, further suppressing chain exchange and coalescence, and stabilizing the coacervate droplets. When the PDEGA block became too long, the microdomain aggregation became too compact and too large to be stabilized by the hydrophilic PHPA block, the block copolymer precipitated from PBS, and a liquid-to-solid phase transition was observed. The key to controlling the coacervate droplet size and its phase transition lies in the tuning of intra- or intermolecular interactions in solution. In this study, hydrophobicity-driven coacervation of PHPA-based polymers was effectively controlled by adjusting the length of the hydrophobic block. Droplet sizes ranging from about 5 μm to 234 nm were precisely achieved through molecular design. Furthermore, the liquid-to-solid phase transition induced by strong hydrophobic interactions provides insights into the molecular basis of certain diseases.

Thermal Protection of GOx by Coacervate Droplets

Because of their convenient size control and tolerance to pH and salt, coacervates prepared using PHPA-*b*-PDEGA copolymers in PBS hold great potential for applications in cell biomimicry, nanoreactors, and drug/gene delivery. To investigate their potential in delivery systems, encapsulation of various model compounds, including hydrophobic Nile red, cationic methylene blue, and biomacromolecular proteins and enzymes, such as bovine serum albumin (BSA) and glucose oxidase (GOx), was carried out in different coacervate systems. Biomacromolecules were labeled with fluorescein isothiocyanate (FITC) for fluorescence imaging. As shown in Fig. 7(a) and Fig. S18 (in ESI), coacervate droplets formed in the presence of 0.5 mg/mL of the model compounds at temperature higher than T_{cp} (35 °C), and all the model compounds were successfully encapsulated inside the droplets as observed by the fluorescent microscopy. The distinct color contrast between the coacervate phase and surrounding medium in Fig. 7(a) indicates a high degree of encapsulation efficiency. To further quantify this capability, the encapsulation efficiencies of the model compounds in the $PHPA_{44}$, $PHPA_{44}$-*b*-$PDEGA_{40}$ coacervate droplets, and $PHPA_{44}$-*b*-$PDEGA_{140}$ precipitates were evaluated. As shown in Fig. 7(b), the encapsulation efficiency of small molecules is usually higher than 80%, regardless of whether they are encapsulated coacervates or precipitates. The high absorption capacity of the $PHPA_{44}$-*b*-$PDEGA_{140}$ precipitates did not differ from that of the coacervate droplets, and the corresponding fluorescence image is shown in Fig. S19 (in ESI). However, the encapsulation efficiency of biomacromolecules (FITC-BSA and FITC-GOx) was significantly lower (no more than 50%), probably because of the absence of ionizable functional groups required for electrostatic interactions,[71] as well as random encapsulation driven by weak interactions between biomacromolecules and PHPA-based polymers. For FITC-BSA and FITC-GOx, the highest encapsulation efficiency was found in the $PHPA_{44}$ coacervate and the lowest in the precipitates, especially

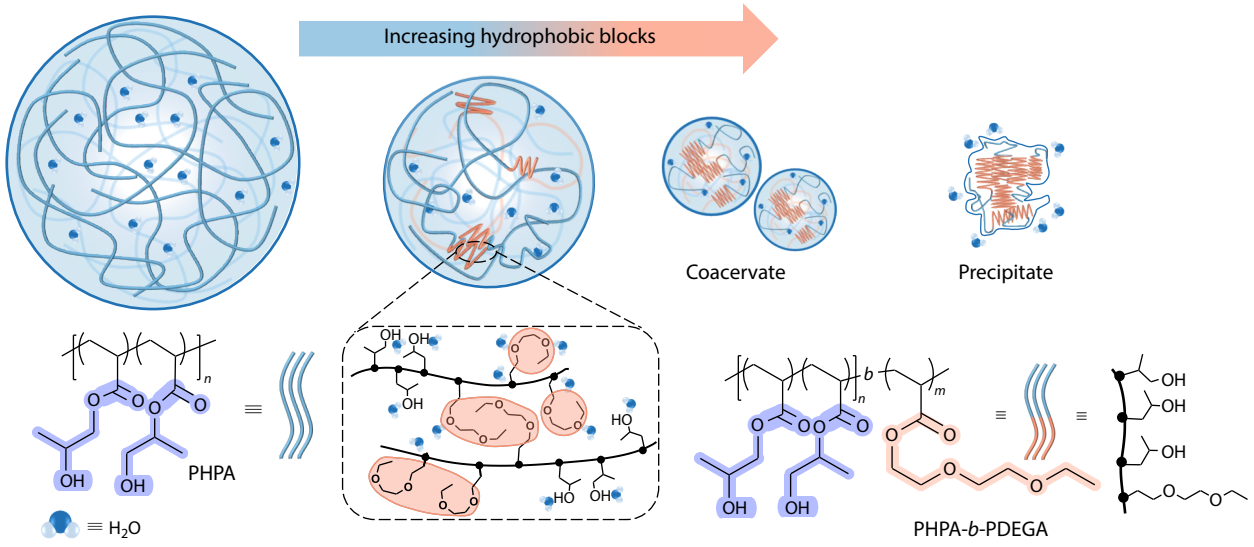

Scheme 3 Schematic illustration of hydrophobicity-regulated size control and liquid-to-solid phase transition in PHPA-*b*-PDEGA copolymers.

https://doi.org/10.1007/s10118-026-3589-6

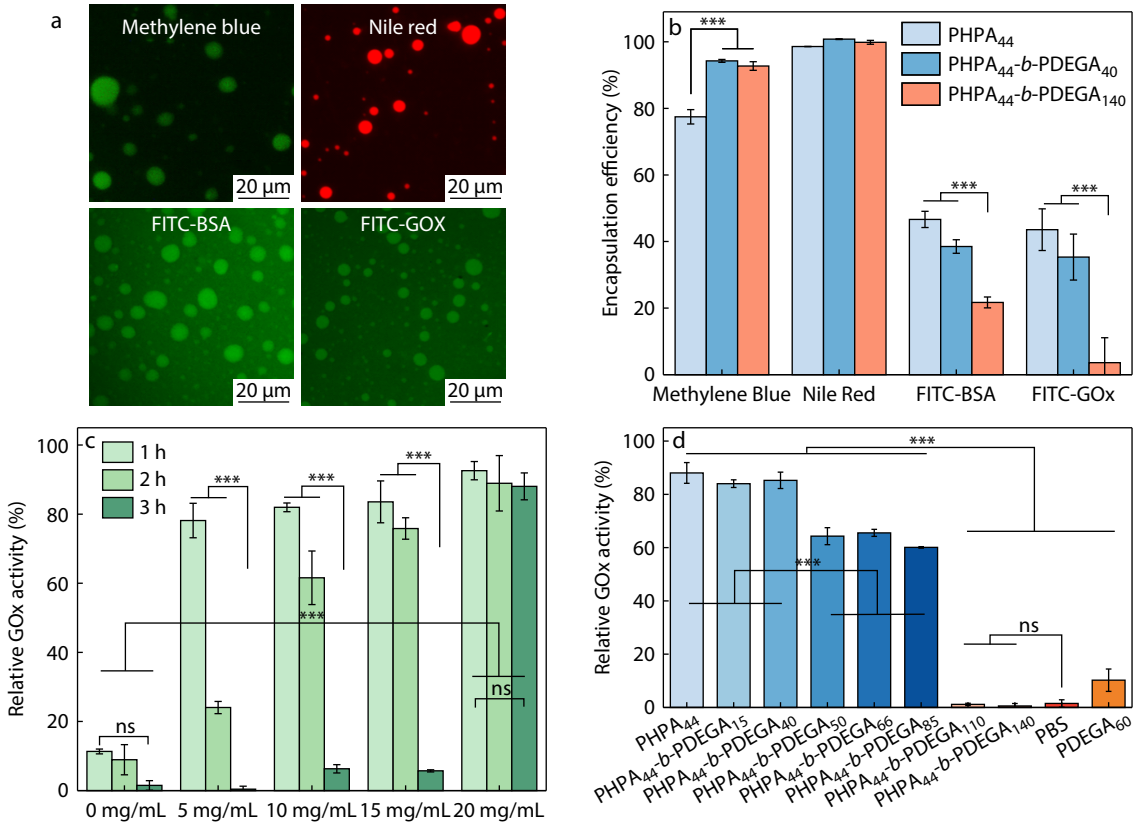

Fig. 7 Encapsulation and thermal protection of GOx by coacervate droplets. (a) Fluorescence microscopy images of $PHPA_{44}$-*b*-$PDEGA_{15}$ coacervates (20 mg/mL, above T_{cp}) in the presence of 0.5 mg/mL methylene blue, Nile red, FITC-BSA, and FITC-GOx, respectively; (b) Encapsulation efficiency of different model compounds by $PHPA_{44}$, $PHPA_{44}$-*b*-$PDEGA_{40}$ coacervates, and $PHPA_{44}$-*b*-$PDEGA_{140}$ precipitates in PBS; (c) Relative GOx activity after thermal treatment at 60 °C (1, 2, and 3 h) protected by $PHPA_{44}$ coacervate at varying concentrations. (d) Relative GOx activity after thermal treatment (60 °C, 3 h) protected by $PHPA_{44}$-*b*-$PDEGA_m$ coacervates (m=0, 15, 40, 50, 66, and 85) and precipitates ($PHPA_{44}$-*b*-$PDEGA_{110}$, $PHPA_{44}$-*b*-$PDEGA_{140}$, and $PDEGA_{60}$) at 20 mg/mL, $^{*}p<0.05$, $^{**}p<0.01$, and $^{***}p<0.001$.

for FITC-GOx (5%). This much lower encapsulation efficiency in the precipitate state is likely due to the highly dehydrated microenvironment within these precipitates, which is unfavorable for hydrophilic BSA and GOx macromolecules. Hence, owing to the neutral and salt-stable properties of these coacervates, a broad range of compounds, including hydrophobic and neutral small molecules, hydrophilic and charged small molecules, and biomacromolecules, can be effectively encapsulated, particularly in the coacervate state, which is particularly advantageous for macromolecules.

It is well known that enzymes play crucial roles in mediating most metabolic processes within living organisms. However, their catalytic activity is extremely sensitive to external stimuli up to the complete loss of catalytic activity. GOx, a temperature- and pH-sensitive enzyme, can be easily denatured at elevated temperatures.[52] In this study, LCST-type coacervation was explored for the thermal protection of GOx. As shown in Fig. 7(c), the relative catalytic activity of GOx after thermal incubation was significantly higher in the presence of the $PHPA_{44}$ coacervate than in pure PBS. Increasing the $PHPA_{44}$ concentration gradually improved the GOx activity and prolonged the thermal tolerance from 1 h (5 mg/mL, 78%) to at least 3 h (20 mg/mL, 88%). As the droplet size of the coacervate increased with concentration, the protection efficiency of GOx likely correlated with the droplet size. Compared to our previous study,[52] this work demonstrates an enhanced ability to protect GOx from thermal treatment, extending the protection duration from 1 h to 3 h, thereby providing improved thermal stability. Thermal protection was further studied using DLS. Without coacervate protection, GOx exhibited a dramatic increase in D_h from 7.3 nm (untreated) to 283 nm (thermally treated) (Fig. S20a in ESI), confirming the irreversible aggregation and enzymatic inactivation at elevated temperatures.[18] In contrast, the $PHPA_{44}$/GOx complex maintained a D_h of 1708 nm, nearly identical to that of the pure $PHPA_{44}$ coacervate (Fig. S20b in ESI), demonstrating that spatial confinement with coacervates restricts GOx aggregation, thereby preserving the enzyme activity.[18] The GOx catalytic activity protected by coacervates was higher than the encapsulation efficiency, probably because of the rapid exchange of GOx between the two liquid phases. As shown in Fig. S21 (in ESI), the coacervate droplets turn green immediately after the addition of trace amounts of FITC-GOx, verifying the transient and dynamic exchange of GOx between the coacervate droplets and the surrounding solution, which mimics the matter and energy exchange functionality of MLOs.[72–74] As a result, all GOx molecules in the solution remained highly active after thermal stress.

Thermal protection of GOx was also evaluated in coacervates with different droplet sizes at 20 mg/mL. As shown in

https://doi.org/10.1007/s10118-026-3589-6

Fig. 7(d), the activity of GOx after 3 h of thermal treatment at 60 °C decreased gradually with reduction in the coacervate droplet size owing to the increasing PDEGA block length. In the $PHPA_{60}$-*b*-$PDEGA_x$ coacervate system, a decrease in thermal protection capability due to the reduction in droplet size can also be observed (Fig. S22 in ESI). Notably, the catalytic activity of GOx dropped dramatically to approximately 1% in the precipitates ($PHPA_{44}$-*b*-$PDEGA_{110}$ and $PHPA_{44}$-*b*-$PDEGA_{140}$), which was lower than that in pure PBS, indicating complete enzymatic inactivation. These results verified that the precipitates adsorbed GOx on their surfaces rather than encapsulating it, as discussed earlier. It is noted that the relative GOx activity of $PDEGA_{60}$ is *ca.* 10%, which is probably due to the random encapsulation of GOx in the $PDEGA_{60}$ precipitates when the temperature was increased above the LCST. As previously reported,[18,75] water-rich coacervate droplets can mimic the natural cellular environment to stabilize biomolecules and prevent their irreversible aggregation and denaturation at high temperatures. Concurrently, the rapid and reversible exchange of GOx between the interior of the coacervate droplets and bulk solution ensures that all enzyme molecules are protected.[76,77] However, precipitates resulting from the liquid-to-solid phase transition cannot provide such a hydrated and dynamic environment, leading to enzyme denaturation. Compared to the high activity retained in LLPS-derived coacervates, the inactivation of GOx in precipitates formed by liquid-to-solid phase transition mimics the pathological mechanisms observed in certain diseases, such as the abnormal deposition of β-amyloid protein (Aβ) in Alzheimer's disease.[78,79]

CONCLUSIONS

In summary, LCST-type thermoresponsive and neutral block copolymers (PHPA-*b*-PDEGA) with varying block lengths, along with their corresponding homopolymers, were synthesized to study the effects of polymer composition and hydrophobic interactions on phase separation behavior in PBS (physiological conditions). At temperatures higher than T_{cp}, LLPS was observed for most polymers in PBS, showing minimal sensitivity to pH or salt concentration. Hydrophobic interactions were identified as the driving force for LLPS, as confirmed by 1,6-hexanediol disruption results. Optical microscopy images and DLS analysis of the $PHPA_{44}$-*b*-$PDEGA_m$ (m=0, 15, 40, 50, 66, and 85) polymers demonstrated that the coacervate droplet sizes gradually decreased from about 5 μm to about 234 nm. Furthermore, a liquid-to-solid phase transition was observed at PDEGA DPs of 110 and 140, accompanied by a lower water content in the precipitate compared to the coacervate phase. The temperature-dependent ^{1}H NMR and 2D NOESY results confirmed that the hydrophobic interactions of the PDEGA block play a crucial role in droplet size control and liquid-to-solid phase transition. As the DP of the PDEGA block increased, the intra- and inter-hydrophobic interactions intensified, forming aggregated microdomains within the coacervate droplets, thereby reducing their size. When the hydrophobic interactions became sufficiently strong, the aggregated microdomains grew large enough to precipitate, resulting in a liquid-to-solid phase transition. The precise size control of coacervate droplets facilitates biomimetic applications. These coacervate droplets can encapsulate both neutral and charged small molecules as well as biomacromolecules, making them promising vehicles for drug/gene delivery. Furthermore, the LCST-type coacervates provided excellent thermal protection for the GOx enzyme because of the rapid and dynamic GOx exchange between the two liquid phases, which functioned as MLOs. The hydrophobicity-regulated control of coacervate droplet size is essential for bio-applications, and insights into the molecular mechanism of liquid-to-solid phase transition offer valuable clues for better understanding the pathological processes in certain diseases.

Conflict of Interests

The authors declare no interest conflict.

Electronic Supplementary Information

Electronic supplementary information (ESI) is available free of charge in the online version of this article at http://doi.org/10.1007/s10118-026-3589-6.

Data Availability Statement

The data that support the findings of this study are available from the corresponding author upon reasonable request.

ACKNOWLEDGMENTS

This study was financially supported by the National Natural Science Foundation of China (No. 52073201).

REFERENCES

1 Brangwynne, C. P.; Eckmann, C. R.; Courson, D. S.; Rybarska, A.; Hoege, C.; Gharakhani, J.; Jülicher, F.; Hyman, A. A. Germline P granules are liquid droplets that localize by controlled dissolution/condensation. *Science* **2009**, *324*, 1729–1732.
2 Lafontaine, D. L. J.; Riback, J. A.; Bascetin, R.; Brangwynne, C. P. The nucleolus as a multiphase liquid condensate. *Nat. Rev. Mol. Cell Biol.* **2020**, *22*, 165–182.
3 Giudice, J.; Jiang, H. Splicing regulation through biomolecular condensates and membraneless organelles. *Nat. Rev. Mol. Cell Biol.* **2024**, *25*, 683–700.
4 Zwicker, D.; Seyboldt, R.; Weber, C. A.; Hyman, A. A.; Jülicher, F. Growth and division of active droplets provides a model for protocells. *Nat. Phys.* **2016**, *13*, 408–413.
5 Shin, Y.; Brangwynne, C. P. Liquid phase condensation in cell physiology and disease. *Science* **2017**, *357*, eaaf4382.
6 Brady, J. P.; Farber, P. J.; Sekhar, A.; Lin, Y.-H.; Huang, R.; Bah, A.; Nott, T. J.; Chan, H. S.; Baldwin, A. J.; Forman-Kay, J. D.; Kay, L. E. Structural and hydrodynamic properties of an intrinsically disordered region of a germ-cell-specific protein on phase separation. *Proc. Natl. Acad. Sci. U. S. A.* **2017**, *114*, E8194–E8203.
7 Yang, S.; Yu, Y.; Jo, S.; Lee, Y.; Son, S.; Lee, K. H. Calcium ion-triggered liquid-liquid phase separation of silk fibroin and spinning through acidification and shear stress. *Nat. Commun.* **2024**, *15*, 10394.
8 Li, P.; Banjade, S.; Cheng, H.; Kim, S.; Chen, B.; Guo, L.; Llaguno, M.; Hollingsworth, J. V.; King, D. S.; Banani, S. F.; Russo, P. S.; Jiang, Q.-

Graphical Abstract

Hydrophobicity Regulated Coacervate Droplet Size and the Thermal Protection Against Denaturation of Enzyme

Ming-Zhe Zhao, Kong-Ying Zhu, Xiao-Yan Yuan, and Li-Xia Ren

Tianjin University

A strategy for regulating the coacervate droplet size and inducing a liquid-to-solid phase transition was developed. As the hydrophobic block length increases, the droplet size decreases, eventually leading to precipitation, accompanied by reduced thermal protection by glucose oxidase. This insight advances size-controllable biomimetic system design and disease-related phase transition understanding.

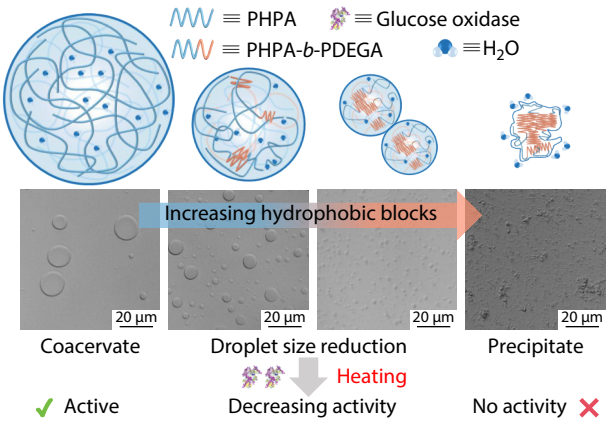

Chinese J. Polym. Sci., 2026 *https://doi.org/10.1007/s10118-026-3589-6*

X.; Nixon, B. T.; Rosen, M. K. Phase transitions in the assembly of multivalent signalling proteins. *Nature* **2012**, *483*, 336–340.

9 Li, Y. X.; Liu, Y. Z.; Yu, X. Y.; Xu, Y.; Pan, X. B.; Sun, Y.; Wang, Y. L.; Song, Y. H.; Shen, Z. Y. Membraneless organelles in health and disease: exploring the molecular basis, physiological roles and pathological implications. *Signal Transduct. Target. Ther.* **2024**, *9*, 305.

10 Xie, F.; Zhou, X.; Ran, Y.; Li, R.; Zou, J.; Wan, S.; Su, P.; Meng, X.; Yan, H.; Lu, H.; Ru, H.; Hu, H.; Mao, Z.; Yang, B.; Zhou, F.; Zhang, L. Targeting FOXM1 condensates reduces breast tumour growth and metastasis. *Nature* **2025**, *638*, 1112–1121.

11 Bal, S.; Gupta, S.; Mahato, C.; Das, D. Catalytically active coacervates sustained out-of-equilibrium. *Angew. Chem. Int. Ed.* **2025**, *64*, e202505296.

12 Abbas, M.; Lipiński, W. P.; Nakashima, K. K.; Huck, W. T. S.; Spruijt, E. A short peptide synthon for liquid–liquid phase separation. *Nat. Chem.* **2021**, *13*, 1046–1054.

13 Kuroyanagi, S.; Shimada, N.; Fujii, S.; Furuta, T.; Harada, A.; Sakurai, K.; Maruyama, A. Highly ordered polypeptide with UCST phase separation behavior. *J. Am. Chem. Soc.* **2018**, *141*, 1261–1268.

14 Morrison, C. A.; Chan, E. P.; Lee, T.; Deming, T. J. Switchable coacervate formation *via* amino acid functionalization of poly(dehydroalanine). *Biomacromolecules* **2024**, *25*, 2554–2562.

15 Scott, W. A.; Benavides, I.; Deming, T. J. Influence of side-chain molecular features on aqueous coacervation of multifunctional homopolypeptides. *Polym. Sci. Technol.* **2024**, *1*, 65–72.

16 Wang, D.; Zhou, L.; Zhang, X.; Zhou, Z.; Huang, Z.; Gao, N. Supramolecular switching of liquid-liquid phase separation for orchestrating enzyme kinetics. *Angew. Chem. Int. Ed.* **2025**, *64*, e202422601.

17 Chowdhury, P.; Saha, B.; Bauri, K.; Sumerlin, B. S.; De, P. Hydrogen bonding-driven self-coacervation of nonionic homopolymers for stimuli-triggered therapeutic release. *J. Am. Chem. Soc.* **2024**, *146*, 21664–21676.

18 Zheng, X.; Wen, L.; Xiao, Y.; Lang, M. Thermo-sensitive polycaprolactone coacervates for preventing protein aggregation under thermal stress. *J. Mater. Chem. B* **2025**, *13*, 2520–2532.

19 Zhang, Z.; Li, H.; Kasmi, S.; Van Herck, S.; Deswarte, K.; Lambrecht, B. N.; Hoogenboom, R.; Nuhn, L.; De Geest, B. G. A synthetic, transiently thermoresponsive homopolymer with UCST behaviour within a physiologically relevant window. *Angew. Chem. Int. Ed.* **2019**, *58*, 7866–7872.

20 Zhao, J.; Hu, Y.; Li, H.; Liu, C.; Nie, Z.; Chen, Z.; Ling, Q.; Li, Z.; Zhao, P.; Song, B.; Zhang, K.; Bian, L. Liquid-liquid phase separation-mediated cellular-scale compartmentalization of hydrogel covalent cross-linking promotes microtubule-based mechanosensing. *J. Am. Chem. Soc.* **2025**, *147*, 14336–14347.

21 Chen, M.; Liu, G.; Zhang, M.; Li, Y.; Hong, X.; Yang, H. Programmatically dynamic microcompartmentation in coacervate-in-pickering emulsion protocell. *Small* **2022**, *19*, 2206437.

22 Swanson, J. P.; Monteleone, L. R.; Haso, F.; Costanzo, P. J.; Liu, T.; Joy, A. A library of thermoresponsive, coacervate-forming biodegradable polyesters. *Macromolecules* **2015**, *48*, 3834–3842.

23 Kim, S.; Lee, M.; Lee, W. B.; Choi, S. H. Ionic-group dependence of polyelectrolyte coacervate phase behavior. *Macromolecules* **2021**, *54*, 7572–7581.

24 Zhao, C.; Wang, X.; Li, L.; Huang, H.; Wu, B.; Zhang, L.; Huang, X. Biomineralization-inspired membranization toward structural enhancement of coacervate community. *Adv. Sci.* **2025**, *12*, 2417832.

25 Hong, Y.; Yoo, S.; Han, J.; Kim, J.; Lee, Y.; Jho, Y.; Kim, Y. S.; Hwang, D. S. Influence of the backbone chemistry and ionic functional groups of five pairs of oppositely charged polyelectrolytes on complex coacervation. *Commun. Chem.* **2024**, *7*, 182.

26 Liu, X. F.; Zhang, C. R.; Peng, H. W.; Zhao, Q. Cation-dipole interaction-induced coacervate underwater adhesives in natural seawater. *Chinese J. Polym. Sci.* **2024**, *42*, 984–991.

27 Li, F.; Lin, Y.; Qiao, Y. Regulating FUS liquid-liquid phase separation *via* specific metal recognition. *Chinese J. Polym. Sci.* **2022**, *40*, 1043–1049.

28 Biswas, S.; Hecht, A. L.; Noble, S. A.; Huang, Q.; Gillilan, R. E.; Xu, A.

Y. Understanding the impacts of molecular and macromolecular crowding agents on protein-polymer complex coacervates. *Biomacromolecules* **2023**, *24*, 4771–4782.
29 Mu, W.; Jia, L.; Zhou, M.; Wu, J.; Lin, Y.; Mann, S.; Qiao, Y. Superstructural ordering in self-sorting coacervate-based protocell networks. *Nat. Chem.* **2024**, *16*, 158–167.
30 Harris, R.; Berman, N.; Lampel, A. Coacervates as enzymatic microreactors. *Chem. Soc. Rev.* **2025**, *54*, 4183–4199.
31 Hassan, L. F.; Sen, R.; O'Shea, T. M. Trehalose-based coacervates for local bioactive protein delivery to the central nervous system. *Biomaterials* **2024**, *309*, 122594.
32 Zhou, L.; Fan, Y.; Liu, Z.; Chen, L.; Spruijt, E.; Wang, Y. A multiresponsive transformation between surfactant-based coacervates and vesicles. *CCS Chem.* **2021**, *3*, 358–366.
33 Wang, D.; Zhang, P.; Zhong, Q. Z.; Liu, H.; Yu, Q.; Gao, N.; Hao, J.; Cui, J. Hydrogen bonding-driven adaptive coacervates as protocells. *ACS Appl. Mater. Interfaces* **2025**, *17*, 6095–6102.
34 Liu, H.; Zhang, P.; Geng, H.; Yang, Z.; Gao, Z.; Wang, N.; You, Y.; Xu, L.; Liu, X.; Zhao, Y.; Cui, J. Full-active-ingredient nanoparticles loaded with salmon calcitonin potentiate antioxidation and lubrication for osteoarthritis therapy. *Chem. Eng. J.* **2025**, *524*, 169456.
35 Phair, R. D.; Misteli, T. High mobility of proteins in the mammalian cell nucleus. *Nature* **2000**, *404*, 604–609.
36 Malatesta, M.; Gazzanelli, G.; Battistelli, S.; Martin, T. E.; Amalric, F.; Fakan, S. Nucleoli undergo structural and molecular modifications during hibernation. *Chromosoma* **2000**, *109*, 506–513.
37 Brangwynne, C. P.; Mitchison, T. J.; Hyman, A. A. Active liquid-like behavior of nucleoli determines their size and shape in *Xenopus laevis* oocytes. *Proc. Natl. Acad. Sci. U. S. A.* **2011**, *108*, 4334–4339.
38 Ponti, D. The nucleolus: a central hub for ribosome biogenesis and cellular regulatory signals. *Int. J. Mol. Sci.* **2025**, *26*, 4174.
39 Weber, S. C.; Brangwynne, C. P. Inverse size scaling of the nucleolus by a concentration-dependent phase transition. *Curr. Biol.* **2015**, *25*, 641–646.
40 Sun, Y.; Wu, X.; Shen, K.; Guo, K.; Lim, D. S.; Chew, W. L.; Yu, J.; Miserez, A. Polyethylene-glycol-conjugated peptide coacervates with tunable size for intracellular mRNA delivery. *ACS Nano* **2025**, *19*, 24724–24735.
41 Allahyartorkaman, M.; Chan, T. H.; Chen, E. H.; Ng, S. T.; Chen, Y. A.; Wen, J. K.; Ho, M. R.; Yen, H. Y.; Kuan, Y. S.; Kuo, M. H.; Chen, R. P. Phosphorylation-induced self-coacervation versus RNA-assisted complex coacervation of tau proteins. *J. Am. Chem. Soc.* **2025**, *147*, 10172–10187.
42 Ren, T. H.; Liang, D. H. Polyelectrolyte complexes and coacervates formed by *De novo*-designed peptides and oligonucleotide. *Chinese J. Polym. Sci.* **2024**, *42*, 1333–1340.
43 Nott, Timothy J.; Petsalaki, E.; Farber, P.; Jervis, D.; Fussner, E.; Plochowietz, A.; Craggs, T. D.; Bazett-Jones, David P.; Pawson, T.; Forman-Kay, Julie D.; Baldwin, Andrew J. Phase transition of a disordered nuage protein generates environmentally responsive membraneless organelles. *Mol. Cell* **2015**, *57*, 936–947.
44 Lin, Y.; Protter, David S. W.; Rosen, Michael K.; Parker, R. Formation and maturation of phase-separated liquid droplets by RNA-binding proteins. *Mol. Cell* **2015**, *60*, 208–219.
45 Zhang, H.; Elbaum-Garfinkle, S.; Langdon, E. M.; Taylor, N.; Occhipinti, P.; Bridges, A. A.; Brangwynne, C. P.; Gladfelter, A. S. RNA controls polyQ protein phase transitions. *Mol. Cell* **2015**, *60*, 220–230.
46 Patel, A.; Lee, Hyun O.; Jawerth, L.; Maharana, S.; Jahnel, M.; Hein, Marco Y.; Stoynov, S.; Mahamid, J.; Saha, S.; Franzmann, Titus M.; Pozniakovski, A.; Poser, I.; Maghelli, N.; Royer, Loic A.; Weigert, M.; Myers, Eugene W.; Grill, S.; Drechsel, D.; Hyman, Anthony A.; Alberti, S. A liquid-to-solid phase transition of the ALS protein FUS accelerated by disease mutation. *Cell* **2015**, *162*, 1066–1077.
47 Yan, X.; Kuster, D.; Mohanty, P.; Nijssen, J.; Pombo-Garcia, K.; Garcia Morato, J.; Rizuan, A.; Franzmann, T. M.; Sergeeva, A.; Ly, A. M.; Liu, F.; Passos, P. M.; George, L.; Wang, S. H.; Shenoy, J.; Danielson, H. L.; Ozguney, B.; Honigmann, A.; Ayala, Y. M.; Fawzi, N. L.; Dickson, D. W.; Rossoll, W.; Mittal, J.; Alberti, S.; Hyman, A. A. Intra-condensate demixing of TDP-43 inside stress granules generates pathological aggregates. *Cell* **2025**, *188*, 4123–4140.
48 Shen, Y.; Chen, A.; Wang, W.; Shen, Y.; Ruggeri, F. S.; Aime, S.; Wang, Z.; Qamar, S.; Espinosa, J. R.; Garaizar, A.; St George-Hyslop, P.; Collepardo-Guevara, R.; Weitz, D. A.; Vigolo, D.; Knowles, T. P. J. The liquid-to-solid transition of FUS is promoted by the condensate surface. *Proc. Natl. Acad. Sci. U. S. A.* **2023**, *120*, e2301366120.
49 Chen, F.; Lu, G.; Yuan, H.; Li, R.; Nie, J.; Zhao, Y.; Shu, X.; Zhu, X. Mechanism and regulation of LCST behavior in poly(hydroxypropyl acrylate)-based temperature-sensitive hydrogels. *J. Mater. Chem. A* **2022**, *10*, 18235–18247.
50 Vancoillie, G.; Frank, D.; Hoogenboom, R. Thermo-responsive poly(oligo(ethylene glycol) acrylates). *Prog. Polym. Sci.* **2014**, *39*, 1074–1095.
51 Vo, C. D.; Rosselgong, J.; Armes, S. P.; Tirelli, N. Stimulus-responsive polymers based on 2-hydroxypropyl acrylate prepared by RAFT polymerization. *J. Polym. Sci., Part A: Polym. Chem.* **2010**, *48*, 2032–2043.
52 Li, Z.; Zhu, K.; Ren, L.; Yuan, X. Sulfonium-containing glycopolypeptides tethering trehalose for protein stabilization. *ACS Macro Lett.* **2022**, *11*, 1278–1284.
53 Hong, X.; Liu, S.; Pang, J.; Zhao, J.; Zhang, G. Polyglycidamides: from backbone-promoted amidation to degradable polyether with wide-range LCST. *Angew. Chem. Int. Ed.* **2025**, *64*, e202419978.
54 Wang, K.; Liu, X. F.; Li, Z. Y.; Zhao, F.; Liu, G. Y.; Zeng, Y. F. New family of multistimuli-responsive acrylamide-based homopolymers: synthesis, responsive behavior, and application in controlled release. *Macromolecules* **2025**, *58*, 5208–5219.
55 Choi, J.; Koo, B.; Kim, C.; Jang, W. D. Thermo-responsive poly(2-isopropyl-2-oxazoline)-based bottlebrush polymers *via* cascade enyne metathesis polymerization. *Macromol. Rapid Commun.* **2025**, *46*, e2500021.
56 Chen, H.; Bao, Y.; Li, X.; Chen, F.; Sugimura, R.; Zeng, X.; Xia, J. Cell surface engineering by phase-separated coacervates for antibody display and targeted cancer cell therapy. *Angew. Chem. Int. Ed.* **2024**, *63*, e202410566.
57 Bao, Y.; Chen, H.; Xu, Z.; Gao, J.; Jiang, L.; Xia, J. Photo-responsive phase-separating fluorescent molecules for intracellular protein delivery. *Angew. Chem. Int. Ed.* **2023**, *62*, e202307045.
58 Liu, X.; Shi, Z.; Yu, F.; Teng, C.; Zhang, C.; Chen, Z. R. The correlation between thermally induced precipitate-to-coacervate transition and glass transition in a polyelectrolyte-bolaamphiphile complex. *Aggregate* **2023**, *4*, e363.
59 Cakmak, F. P.; Choi, S.; Meyer, M. O.; Bevilacqua, P. C.; Keating, C. D. Prebiotically relevant low polyion multivalency can improve functionality of membraneless compartments. *Nat. Commun.* **2020**, *11*, 5949.
60 Neitzel, A. E.; Fang, Y. N.; Yu, B.; Rumyantsev, A. M.; de Pablo, J. J.; Tirrell, M. V. Polyelectrolyte complex coacervation across a broad range of charge densities. *Macromolecules* **2021**, *54*, 6878–6890.
61 Sabari, B. R.; Dall'Agnese, A.; Boija, A.; Klein, I. A.; Coffey, E. L.; Shrinivas, K.; Abraham, B. J.; Hannett, N. M.; Zamudio, A. V.; Manteiga, J. C.; Li, C. H.; Guo, Y. E.; Day, D. S.; Schuijers, J.; Vasile, E.; Malik, S.; Hnisz, D.; Lee, T. I.; Cisse, I. I.; Roeder, R. G.; Sharp, P. A.; Chakraborty, A. K.; Young, R. A. Coactivator condensation at super-enhancers links phase separation and gene control. *Science* **2018**, *361*, eaar3958.

62 Xie, X.; Li, T.; Ma, L.; Wu, J.; Qi, Y.; Yang, B.; Li, Z.; Yang, Z.; Zhang, K.; Chu, Z.; Ngai, T.; Xia, J.; Wang, Y.; Zhao, P.; Bian, L. A designer minimalistic model parallels the phase-separation-mediated assembly and biophysical cues of extracellular matrix. *Nat. Chem.* **2025**, *17*, 1216–1226.

63 Xu, M.; Qi, Y.; Liu, G.; Song, Y.; Jiang, X.; Du, B. Size-dependent *in vivo* transport of nanoparticles: implications for delivery, targeting, and clearance. *ACS Nano* **2023**, *17*, 20825–20849.

64 Walkey, C. D.; Olsen, J. B.; Guo, H.; Emili, A.; Chan, W. C. Nanoparticle size and surface chemistry determine serum protein adsorption and macrophage uptake. *J. Am. Chem. Soc.* **2012**, *134*, 2139–2147.

65 Jin, H.; Heller, D. A.; Sharma, R.; Strano, M. S. Size-dependent cellular uptake and expulsion of single-walled carbon nanotubes: single particle tracking and a generic uptake model for nanoparticles. *ACS Nano* **2009**, *3*, 149–158.

66 Hou, L.; Wu, P. LCST transition of PNIPAM-*b*-PVCL in water: cooperative aggregation of two distinct thermally responsive segments. *Soft Matter* **2014**, *10*, 3578–3586.

67 Lutz, J. F. Polymerization of oligo(ethylene glycol) (meth)acrylates: toward new generations of smart biocompatible materials. *J. Polym. Sci., Part A: Polym. Chem.* **2008**, *46*, 3459–3470.

68 Swanson, J. P.; Martinez, M. R.; Cruz, M. A.; Mankoci, S. G.; Costanzo, P. J.; Joy, A. A coacervate-forming biodegradable polyester with elevated LCST based on bis-(2-methoxyethyl)amine. *Polym. Chem.* **2016**, *7*, 4693–4702.

69 Deng, Y.; Chen, B.; Zhu, K.; Ren, L.; Yuan, X. Activation of upper critical solution temperature behaviors of zwitterionic poly($_L$-methionine-*g*-poly(sulfobetaine methacrylate)$_m$) with a bottlebrush structure. *Macromolecules* **2023**, *57*, 191–200.

70 Li, J.; Zhang, Y.; Zhang, F.; Wang, R.; He, Y.; Song, P. Cyclodextrin-grafted poly(vanillin) antimicrobial bio-nanohoops via "graft from" RAFT and supramolecular host–guest chemistry. *Macromolecules* **2024**, *57*, 11190–11198.

71 Cruz, M. A.; Morris, D. L.; Swanson, J. P.; Kundu, M.; Mankoci, S. G.; Leeper, T. C.; Joy, A. Efficient protein encapsulation within thermoresponsive coacervate-forming biodegradable polyesters. *ACS Macro Lett.* **2018**, *7*, 477–481.

72 Novakovic, M.; Han, Y.; Kathe, N. C.; Ni, Y.; Emmanouilidis, L.; Allain, F. H. T. LLPS REDIFINE allows the biophysical characterization of multicomponent condensates without tags or labels. *Nat. Commun.* **2025**, *16*, 4628.

73 Kim, N.; Yun, H.; Lee, H.; Yoo, J. Y. Interplay between membranes and biomolecular condensates in the regulation of membrane-associated cellular processes. *Exp. Mol. Med.* **2024**, *56*, 2357–2364.

74 Day, K. J.; Kago, G.; Wang, L.; Richter, J. B.; Hayden, C. C.; Lafer, E. M.; Stachowiak, J. C. Liquid-like protein interactions catalyse assembly of endocytic vesicles. *Nat. Cell Biol.* **2021**, *23*, 366–376.

75 McCall, P. M.; Srivastava, S.; Perry, S. L.; Kovar, D. R.; Gardel, M. L.; Tirrell, M. V. Partitioning and enhanced self-assembly of actin in polypeptide coacervates. *Biophys. J.* **2018**, *114*, 1636–1645.

76 Bos, I.; Sprakel, J. Langevin dynamics simulations of the exchange of complex coacervate core micelles: the role of nonelectrostatic attraction and polyelectrolyte length. *Macromolecules* **2019**, *52*, 8923–8931.

77 Zheng, J.; Gao, Q.; Ge, G.; Wu, J.; Tang, C. H.; Zhao, M.; Sun, W. Heteroprotein complex coacervate based on β-conglycinin and lysozyme: dynamic protein exchange, thermodynamic mechanism, and lysozyme activity. *J. Agric. Food Chem.* **2021**, *69*, 7948–7959.

78 Niu, Z.; Gui, X.; Feng, S.; Reif, B. Aggregation mechanisms and molecular structures of amyloid-β in Alzheimer's disease. *Chem. Eur. J.* **2024**, *30*, e202400277.

79 Gui, X.; Feng, S.; Li, Z.; Li, Y.; Reif, B.; Shi, B.; Niu, Z. Liquid-liquid phase separation of amyloid-β oligomers modulates amyloid fibril formation. *J. Biol. Chem.* **2023**, *299*, 102926.

https://doi.org/10.1007/s10118-026-3589-6